Particuology 115 (2026) 68–77

Contents lists available at ScienceDirect

Particuology

journal homepage: www.elsevier.com/locate/partic

An adaptive lattice Boltzmann method for wake effect on drag force of interactive particles in supercritical water

Xue Qiao, Hui Jin, Haozhe Su, Liejin Guo*

State Key Laboratory of Multiphase Flow in Power Engineering (SKLMFPE), Xi'an Jiaotong University, Xi'an, 710049, China

HIGHLIGHTS

- A multi-segment Boussinesq approximation for supercritical water density is employed in the lattice Boltzmann equation to characterize its density variation under supercritical conditions.
- Boudary lattice based on density gradient was developed to ensure stability of simulation.
- Significant enhancement in boundary convergence and adaptability to thermophysical properties of supercritical water using adaptive LBM scheme.
- A correlation was derived to quantify the wake effect on drag force of interactive particles.

GRAPHICAL ABSTRACT

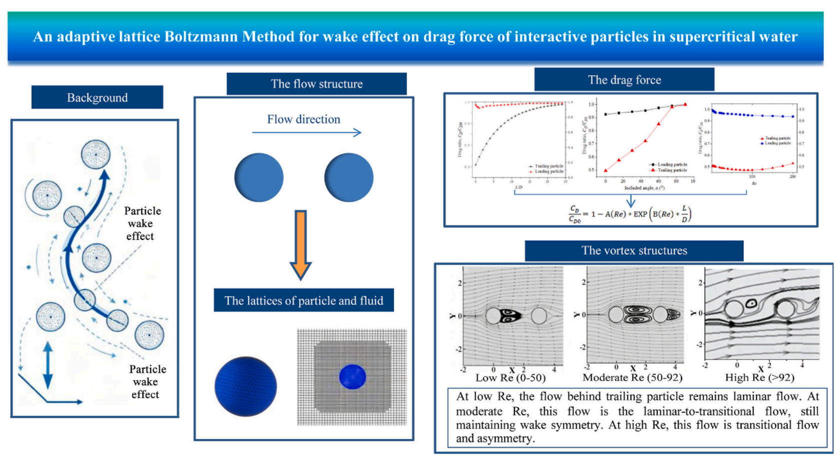

ARTICLE INFO

Keywords:
Lattice Boltzmann method
Boussinesq approximation
Wake effect
Drag force
Numerical simulation

ABSTRACT

Supercritical water gasification (SCWG) is a highly promising technology. A fundamental aspect of SCWG involves the flow of supercritical water (SCW) around interactive particles, which is inherently complex due to the presence of the wake effect. This study numerically investigates particle wake characteristics and wake-particle interactions in high-viscosity supercritical water (SCW) via an adaptive lattice Boltzmann method (LBM, $N/D = 30$, coarse-fine ratio 0.025:0.060) to support supercritical water gasification (SCWG) reactor optimization. The adaptive LBM effectively balances accuracy and efficiency, resolving SCW's steep viscosity gradients and fine wake structures well. Interparticle distance (L/D) is the dominant factor for particle drag, affecting trailing particles far more significantly, with three interaction regimes (strong: $L/D = 0$–2, moderate: 2–4, weak: $\geq$4). SCW's high viscosity amplifies wake overlap at $L/D \leq 2$, minimizing trailing particle pressure drag and suppressing vortex shedding; increasing L/D weakens shielding, elevates drag, and makes trailing particles behave like isolated ones. Interparticle angle raises drag ratios, inducing distinct vortex structures at 30°–60° and 60°–90°, with identical drag at 90°. SCW wake symmetry and vortex shedding show Re-dependent transitions, with critical $Re = 92$ corresponding to the minimum trailing particle drag ratio. A drag ratio correlation with L/D

This article is part of a special issue entitled: Reactive Particle-Gas Systems II published in Particuology.
* Corresponding author.
E-mail address: lj-guo@mail.xjtu.edu.cn (L. Guo).

https://doi.org/10.1016/j.partic.2026.04.026
Received 2 December 2025; Received in revised form 21 April 2026; Accepted 23 April 2026
Available online 12 May 2026

and *Re* is also established. This work provides a reliable numerical tool for SCW particle interactions and theoretical guidance for SCWG reactor optimization, with future work focusing on particle swarms and experimental validation.

1. Introductions

Hydrogen production from coal gasification in the SCWG has advantages, such as high energy efficiency and low environmental pollution (Jin et al., 2010). Supercritical water flow past particles is a fundamental question to design and control of SCWG. However, in general, the drag force and surrounding flow structure of interactive particles are quite different from those of an isolated particle (Chen & Wu, 2000). Hence, the supercritical water flows past two interactive particle deserves to be studied.

Pioneering work is experimental measurement and fluid visualization. Taneda et al. (Taneda, 1956) used pendlum method and water channel flow to take an excellent picture to measure the drag force at a low Reynolds number less than 20. Using the -same method, Tsuji et al. (Tsuji, Morikawa and Terashima, 1982) discussed the vortices of two spherical particles at Reynolds numbers over 200. For fluid visualization, Zhu et al. (Zhu et al., 1994) did an experiment to measure the drag force on two interactive particles at Reynolds numbers of 20–130. However, these studies are primarily applicable to ambient temperature and pressure conditions, not suitable for supercritical water environments.

Due to the high-temperature and high-pressure operating conditions of SCWR, conducting experiments to measure the entire flow field is extremely challenging. Thus, the researches of drag force of particles was mainly simulations (Li et al., 2021; Wang & You, 2011; Zhang et al., 2020).

In recent years, research on the drag force on the particle in supercritical water has been a focus. Wei et al. (Wei, Lu & Wei, 2014) adopted 2D SIMPLEC to simulate drag force on a spherical particle over the Reynolds number range of 10–100. The result showed that when subcritical water flows through a spherical particle, the drag coefficient of the particle will reduce, and a larger vortex will form due to dynamic viscosity. Jin et al. (Jin et al., 2019) numerically studied the drag coefficient and flow characteristics of supercritical water flowing through two solid biomass spherical particles in the range of 10<Re < 200, with the effects of interparticle distance and the angle between particles considered. The results showed that the drag coefficient is mainly affected by the wake region behind the leading particles and the wake effect between particles. Zhang et al. (Zhang et al., 2020) used Fluent 15.0 to analyze the drag force on nonspherical particles under varying conditions. However, these simulation methods are limited to the particle scale and unappliable to up-scaled systems.

Since LBM has many advantages, such as natural parallelism, high computational efficiency, and easy implementation of complex boundaries, LBM demonstrates high efficiency and accuracy in simulating full-scale problems. Recently, LBM has been widely used (Wang et al., 2015; Xiang et al., 2013; Yu & Fan, 2010; Zhang et al., 2021; Zhang, Ozalp; Xie, 2019). Based on this feature, LBM has potentials to deal with the flow problems in supercritical water reactor(SCWR). LBM is widely used in studying fluid flow past interactive particles (Chen & Wu, 2000; Liu et al., 2024; Liu & Guo, 2013; Wu et al., 2012).

Chen and Doolen (1998) used Lattice Boltzmann Equation (LBE) to simulate fluid flow past two interactive particles with different interparticle distances and Reynolds numbers, among which the drag force of the particle cluster is directly calculated by the momentum exchange method.

Zhang and Fan (2002) developed a semi-empirical expression for the drag force of two interactive particle under the wake effect. This expression is suitable for the flow with Reynolds numbers of 54–154.

However, these studies have not obtained a mechanistic correlation to quantify the wake effect on the trailing particle. In this work, we adopted an adaptive Lattice Boltzmann method (LBM) based on multi segment Boussinesq approximation of density to study the flow structure and drag force of the monoparticle system and two particle system at an enlarged Reynolds number of 0.1-1000 and 0.1-200. The aim of this work is to obtain a correlation to quantify the wake effect with a supercritical water environment at 23 MPa and 637.15-727.15K.

2. Simulation method

2.1. Simulation method

The governing equations of the fluid are listed as Eqs. (1) and (2):

$$\nabla \cdot (\rho \boldsymbol{u}) = 0 \tag{1}$$

$$\frac{\partial \rho \boldsymbol{u}}{\partial t} + \nabla \cdot (\rho \boldsymbol{u}\boldsymbol{u}) = -\nabla p + \nu \nabla^2 (\rho \boldsymbol{u}) + \nabla \cdot (\rho \nu \nabla \boldsymbol{u}) \tag{2}$$

However, the density of SCW varies with temperature and pressure (Wagner et al., 2000). Due to the local pressure in SCWR being basically constant when SCWR runs stably (Wei & Lu, 2016), we assumed the density of SCW is a function of temperature. Since that the Boussinesq approximation (Chen & Doolen, 1998) is applicable on the premise that the relative density variation ($\Delta\rho/\rho_0$) is sufficiently small (generally $\Delta\rho/\rho_0$<5% for fluid-particle interaction simulations). For high-viscosity SCW (μ = 0.0012–0.0025 Pa s) in this study, the density variation $\Delta\rho$ induced by flow velocity and temperature gradients is quantitatively calculated as 0.8–3.2 kg/m^3, corresponding to $\Delta\rho/\rho_0$ = 0.4%–1.6% (ρ_0 = 200 kg/m^3, SCW reference density). Thus, we adopt Boussinesq approximation as this function.

Then, the density of SCW can be given by Eq. (3):

$$\rho = \rho_0[1 - \beta(T - T_0)] \tag{3}$$

where β is the thermal expansion coefficient.

The gravitational body force under the Boussinesq approximation can be formulated as Eq. (4):

$$\boldsymbol{G} = \rho_0 \boldsymbol{g}[1 - \beta(T - T_0)] \tag{4}$$

After being divided by ρ_0 and absorbing $\rho_0 \boldsymbol{g}$ into ∇p, the simplified governing equations (Chen & Doolen, 1998) are given by:

$$\nabla \cdot \boldsymbol{u} = 0 \tag{5}$$

$$\frac{\partial \boldsymbol{u}}{\partial t} + \nabla \cdot (\boldsymbol{u}\boldsymbol{u}) = -\frac{\nabla p}{\rho_0} + \nabla \cdot (\nu \nabla \boldsymbol{u}) - \boldsymbol{g}\beta(T - T_0) \tag{6}$$

in the LBM, the flow field is represented on a discrete lattice. Compared with standard LBE, Eq. (5) has an additional gravity term caused by thermal expansion of density. With appropriate boundary conditions and Chapman-Enskog expansion of Eqs. (5) and (6), for a lattice, the lattice velocity distribution function can be assumed as:

$$f_i(\boldsymbol{x} + \boldsymbol{c}_i\delta_t, t + \delta_t) - f_i(\boldsymbol{x}, t) = \frac{(f_i - f^{eq})}{\tau_0} + \Delta t \boldsymbol{F}_i \boldsymbol{F}_\alpha \tag{7}$$

Where τ_0 is the relaxation time toward equilibrium, resulting in the notation relaxation characteristic time (which is related to macroscopic viscosity), $\boldsymbol{x}$ is a grid point in lattice $\boldsymbol{L}$, and $\boldsymbol{L}$ is a self–closed system generally. Thus, $\boldsymbol{x} + \boldsymbol{c}_i\delta_t$ also belongs to lattice $\boldsymbol{L}$, ensuring that particle distributions stream exactly between lattice nodes.

$\boldsymbol{F}_i$ is the external force acting on the lattice, showing as Eq. (5):

$$\boldsymbol{F}_i = \left(1-\frac{1}{2\tau_0}\right)\omega_i\left(\frac{\boldsymbol{\xi}_i-\boldsymbol{u}}{c_s^2}+\frac{\boldsymbol{\xi}_i\cdot\boldsymbol{u}}{c_s^2}\xi_i\right) \tag{8}$$

$\boldsymbol{F}_\alpha$ is the external force exerted by density variation. This force can be written as:

$$\boldsymbol{F}_\alpha = -\beta\boldsymbol{g}(T-T_0) \tag{9}$$

f^{eq} is the equilibrium distribution function. With appropriate boundary conditions, the flow field of SCW can be simulated. The LBM scheme is classified as a function of spatial dimensions d and the number of discrete velocity distribution functions m, abbreviated as $DdQm$ (Chen & Doolen, 1998). In this research, $D2Q9$ is appropriately adopted. Thus, f^{eq} can be written as Eq. (10) according to earlier research (Chen & Doolen, 1998):

$$f_i^{eq} = \omega_i\rho\left(1+3\frac{\boldsymbol{e}_i\cdot\boldsymbol{u}}{c_s}+4.5\frac{(\boldsymbol{e}_i\cdot\boldsymbol{u})^2}{c_s^2}-1.5\frac{|\boldsymbol{u}|^2}{c_s^2}\right) \tag{10}$$

Where c_s is the speed of sound, $\boldsymbol{u}$ is the macroscopic velocity, ρ is the density of supercritical water, ω_i is built as a coefficient to preserve the isotropy in space, and $\omega_0 = 4/9$, $\omega_1 = \omega_2 = \omega_3 = \omega_4 = 1/9$, $\omega_5 = \omega_6 = \omega_7 = \omega_8 = 1/36$. Where $\boldsymbol{e}_i$ is the discrete velocity in the i direction of the lattice, and its expression is as follows:

$$\boldsymbol{e}_i = \begin{cases} (0,0) \; i=0 \\ \left(\cos\left(\frac{\pi(i-1)}{2}\right), \sin\left(\frac{\pi(i-1)}{2}\right)\right) \; i=1,2,3,4 \\ \sqrt{2}\left(\cos\left(\frac{\pi(i-4.5)}{2}\right), \sin\left(\frac{\pi(i-4.5)}{2}\right)\right) \; i=5,6,7,8 \end{cases} \tag{11}$$

While the lattice parameters are derive from the macroscopic physical properties of SCW. The moments of the lattice velocity distribution functions are given as (Chen & Doolen, 1998):

$$\sum f_i = \rho_0, \sum \rho_i \boldsymbol{c}_i = \rho_0\boldsymbol{u}, \sum \rho_i \boldsymbol{c}_i\boldsymbol{c}_i = \sigma \tag{10}$$

Where $\boldsymbol{c}_i$ is the lattice velocity, defined as $\boldsymbol{c}_i = \frac{\Delta x}{\Delta t}$, and Δx is the length of lattice , Δt is the time for this movement. Drag force is an essential element to characterize the flow field, representing the force of the interaction between the particle and fluid. The direction of the drag force is opposite to the direction of the incoming flow. The value of the drag force on a particle can be written as follows:

$$F_D = \frac{1}{2}\rho_f C_D A u_\infty^2 \tag{12}$$

Where C_D is the drag coefficient, u_∞ is the undisturbed field velocity far from the particle. A is the projected area of particles in the direction of incoming flow, namely the maximum sectional area of a spherical particle, known as Eq. (12).

$$A = \frac{1}{4}\pi D^2 \tag{13}$$

where D is the particle diameter. According to Eqs. (8) and (9), at a given Reynolds number, the drag coefficient can be written as:

$$C_D = \frac{F_D}{\frac{1}{4}\pi\rho_f D^2\cdot\frac{1}{2}\rho_p u_\infty^2} \tag{14}$$

Ladd et al. (Ladd, 1994) proposed the momentum exchange method to calculate the interaction force between the particle and fluid at the interactive point, given by:

$$\boldsymbol{f}_i\left(\boldsymbol{x}_b, t+\frac{1}{2}\right) = 2\left(f_i(\boldsymbol{x}_f,t)-f_i(\boldsymbol{x}_p,t)\right)\boldsymbol{c}_i \tag{15}$$

Where $\boldsymbol{x}_b, \boldsymbol{x}_f, \boldsymbol{x}_p$ is the node of the boundary, fluid side, and particle side. This expression is suitable for a stationary boundary with a uniform lattice. Thus, the drag force on a specific particle is written as follows:

$$\boldsymbol{F}_D = \oint_S^i \boldsymbol{f}_i\left(\boldsymbol{x}_b, t+\frac{1}{2}\right) \tag{16}$$

where S is the surface of the particle.

2.2. Boundary condition

For high-viscosity SCW flow past particles, the flow field exhibits distinct spatial inhomogeneity: the near-particle wake zone is dominated by steep viscosity gradients, intense vortex shedding, and strong momentum exchange, requiring high grid resolution to accurately resolve fine-scale wake structures and viscous boundary layers; in contrast, the far-field flow zone has gentle gradients, weak viscous effects, and uniform flow characteristics, where high grid resolution is unnecessary and would only lead to redundant computational cost. However, uniform lattice schemes fail to adapt to this inhomogeneity, and their inherent disadvantages are further amplified by the unique properties of SCW. In sharp contrast, the adaptive LBM framework effectively overcomes these disadvantages by dividing the computational domain into fine lattice regions (near-particle wake zone, where density/velocity gradients are steep) and coarse lattice regions (far-field flow zone), with a refinement ratio of 2:1 between fine and coarse lattices (one coarse grid cell corresponds to four fine grid cells). This design is fully compatible with the spatial inhomogeneity of SCW flow: it ensures high resolution in the near-particle zone to accurately resolve the steep viscosity gradients and wake vortices induced by SCW's high viscosity, while adopting coarse grids in the far field to reduce redundant computational cost.

Thus, multiscale lattices (Filippova et al., 2002; Dupuis & Chopard, 2003; Filippova & Hänel, 2000) are proper to use in this case.

After a comprehensive consideration of the validity and efficiency of the calculations, the computational domain is length $L = 20D$, width $W = 10D$, height $H = 5D$, where D is the particle diameter.

And considering the nearly negligible surface tension of SCW, the inlet adopts a velocity boundary condition, the outlet adopts a pressure boundary condition, and the wall adopts a no-slip boundary condition.

Considering the temperature around the particle is different from that away from the particle because of friction (Tsuji et al., 2003), density can be a factor in deciding the scale of lattices. Assuming the thermal expansion coefficient of lattices for the flow field away from the particle is β_1, and that around the particle is β_2, which can be calculated based on correlations by Wagner et al. (Kretzschmar et al. 2007, 2009; Wagner et al., 2000). Suppose the lattice between coarse lattices and fine lattices is f_{bi}. Then, f_{bi+1} is the coarse neighborhood lattice, and f_{bi-1} is the fine one. According to Eq. (7), f_{bi+1}, f_{bi}, and f_{bi-1} are given by:

$$f_{bi+1} - f_{bi} = \frac{(f_{bi}-f^{eq})}{\tau_0} - \Delta t F_{bi}\beta_1 g(T_{bi+1}-T_{bi}) \tag{17}$$

$$f_{bi} - f_{bi-1} = \frac{(f_{bi-1}-f^{eq})}{\tau_0} - \Delta t F_{bi-1}\beta_2 g(T_{bi}-T_{bi-1}) \tag{18}$$

in this work, we assum the temperature of flow field far from particle is within 637.15-667.15K, and temperature of flow field near the particleis within 667.15-727.15. The lattices of particle surfaces is based on the lattices of flow field to calculate drag force according to Eq. (16). The total number of lattices is 2,400,000, structured grids are adopted, $y^+ < 1$ near the wall, 15 layers are set in the boundary layer, and the growth rate is 1.15. Then, a lattice scheme with coarse lattices in the fluid field and fine lattices in the neighborhood of the particle was arranged as Fig. 1 (a) and (b).

Mass and momentum conservation at coarse-fine lattice interfaces was ensured by a linear interpolation-based distribution function reconstruction method, tailored for high-viscosity SCW flow. The distribution function of coarse grids was averaged from four corresponding

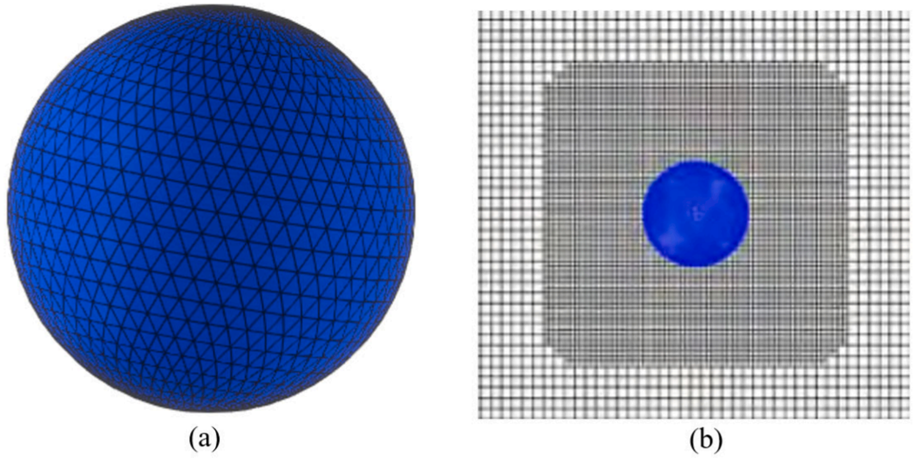

Fig. 1. Lattices of the surface of particle (a) and fluid field (b).

fine grids (0.025:0.060 refinement ratio), while fine grids were interpolated from coarse grids with a viscosity-calibrated correction coefficient (0.98). Post-interpolation validation showed that the relative error of mass conservation at interfaces was <0.1%, and momentum conservation error was <0.3% for $Re = 25$–150 in SCW. Iterative correction was applied if errors exceeded thresholds, eliminating artificial mass/momentum gain/loss and ensuring accurate simulation of wake vortex evolution and drag force in high-viscosity SCW.

2.3. Lattice indepence verification

To ensure the numerical reliability and convergence of the proposed adaptive LBM framework for simulating high-viscosity supercritical water (SCW) flow past particles, a systematic grid independence verification was conducted prior to the formal simulation. The drag coefficient C_D of an isolated particle in SCW (23 MPa, 673.15 K) and key wake structural parameters (wake length, vortex shedding intensity) were selected as the validation indices, covering the core flow characteristics concerned in this study. Three sets of adaptive grid systems with different resolution levels were designed, where the number of lattice nodes per particle diameter (*N/D*) was the core variable for the near-particle fine lattice (matching the adaptive refinement criterion based on density and velocity gradients): Coarse grid: $N/D = 20$ (fine lattice grid size Δxfine $= 0.05D$, coarse lattice Δxcoarse $= 0.12D$); Medium grid: $N/D = 30$ (fine lattice Δxfine $= 0.033D$, coarse lattice Δxcoarse $= 0.0792D$); Fine grid: $N/D = 40$ (fine lattice Δxfine $= 0.025D$, coarse lattice Δxcoarse $= 0.060D$). The refinement ratio between fine and coarse lattices was fixed at 2:1 for all grid systems, consistent with the setting of the adaptive LBM framework. The verification results demonstrated that the medium grid system ($N/D = 30$) achieves an optimal balance between numerical accuracy and computational efficiency, and thus was adopted for all simulation cases in this study.

Lattice independence verification results for the adaptive LBM framework are presented in Fig. 2, where the variation of the isolated particle drag coefficient C_D with the number of lattice nodes per particle diameter (*N/D*) is shown for typical Reynolds numbers 25-150 in SCW. It can be observed that C_D gradually converges with the increase of *N/D*: the relative error of C_D between the coarse grid ($N/D = 20$) and fine grid ($N/D = 40$) ranges from 4.2% to 5.8% for $Re = 25$–150, while the relative error between the medium grid ($N/D = 30$) and fine grid is less than 1.0% for all tested *Re* values. Meanwhile, the wake length and vortex shedding intensity simulated by the medium grid show a deviation of less than 1.2% from the fine grid results (inset of this figure), indicating that the medium grid is sufficient to resolve the steep viscosity gradient and fine-scale wake vortices in high-viscosity SCW. In terms of computational efficiency, the adaptive medium grid reduces the total computational cost by approximately 30% compared with the adaptive fine grid, which is critical for the parametric study of two interacting particles involving multiple working conditions.

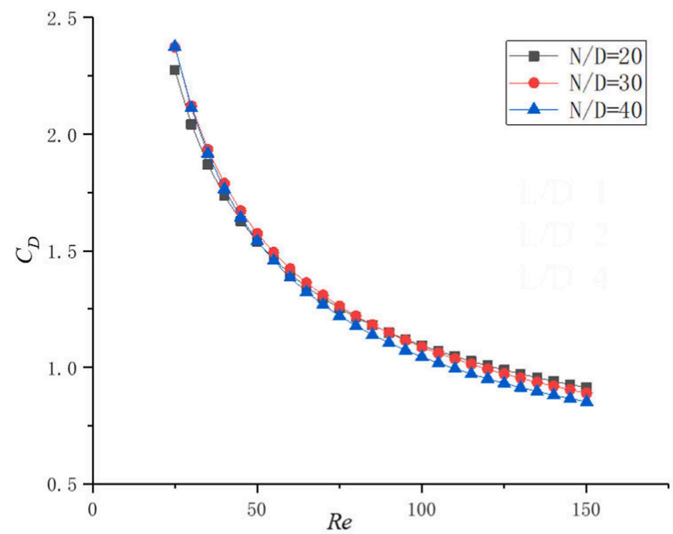

Fig. 2. Drag coefficient of particle (C_D) when $N/D = 20$, 30, 40.

3. Result and discussion

3.1. Validation

How fluid flows through an isolated particle is a typical question of hydrodynamics, which has been well solved. By solving the supercritical water flow through a stationary isolated particle, the accuracy of the LBM model is validated, which is compared with the empirical formula's result and experimental data.

In terms of drag force on a monoparticle, many researchers (Khan & Richardson, 1989) have done productive experiments on it, which have covered a wide range of Reynolds numbers. Among these works, the drag coefficient, which is known as a dimensionless parameter to value the magnitude of the drag force under varying conditions, has been adopted.

Due to supercritical water flow at low Reynolds number in SCWR, a Reynolds number range of 0.1–10000 has been chosen as the range of this study. Clift and Gauvin (1971) gave a comprehensive empirical formula based on published data. Turton and Levenspiel (1986)) noticed that there is a small difference between the experiment and Clift's correlation, so that they improved it. Khan and Richardson (1989) adopted a new approach to analyze data and interpret to obtain a set of correlations.

Fig. 3 displays the comparison between simulation results and experimental correlation. We can see the uniformity of the simulation result with the empirical formulas and experimental data. It is also noticed that the drag coefficient of the particle in the supercritical water is slightly bigger than that in other fluid basically, and when *Re* is bigger, this difference is bigger. That is because the supercritical water has a feature of high dynamic viscosity. Thus, at a specific *Re*, the velocity of supercritical water is bigger than that of a normal fluid.

Fig. 4 checks whether our simulation result is within 90% confidence interval of the experimental data of Khan and Richardson (1989) or not. The result shows a high consistency within this interval on the whole range of Re. Thus, LBM is suitable for the flow field of supercritical water flowing past two particles.

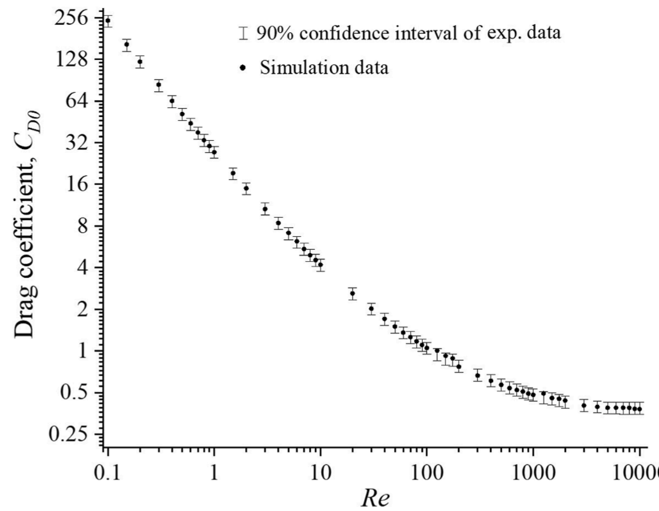

Fig. 4. Drag force as a function of *Re*: simulation data in 90% confidence interval of exp. data (Khan & Richardson, 1989).

3.2. Supercritical water flows past two interacting particles

The high viscosity of SCW enhances viscous dissipation in the particle wake, suppressing vortex diffusion and wake decay, which effectively extends the wake length of the leading particle. This wake extension is closely related to the thermophysical properties of SCW and the flow regime (laminar/transitional), and it further regulates the wake-particle interaction and drag modification of the trailing particle, which is a key difference between SCW and conventional fluid environments in terms of particle wake characteristics. For practical supercritical water gasification (SCWG) engineering, this characteristic is crucial for optimizing the particle motion control and flow field design of reactors, and it can provide theoretical guidance for improving the gasification efficiency and operational stability of SCWG systems for biomass/coal hydrogen production.

Many researchers have studied this condition, such as Zhu et al. (2018) and Chen et al. (Chen & Wu, 2000). According to these studies, it can be concluded that the interparticle distance, interparticle angle α, and Reynolds number $\left(Re = \frac{\rho u D}{\mu}\right.$, where ρ is the denstiy, u is the incoming flow velocity, D is the particle diameter, and μ is the dynamic viscosity) are the fatal factors of the strength of the drag force.

In order to compare the magnitude of the drag force, we choose the drag ratio C_D/C_{D0} as a dimensionless number, where C_D is the drag coefficient on particle in a two-particle system, C_{D0} is the drag coefficient on a monparticle with the same Reynolds number as a two-particle system. The concept of drag ratio was first proposed by Zhu et al. (Zhu et al., 2018). According to this definition, when the drag ratio of the trailing particle becomes smaller, the drag force of the trailing particle becomes smaller than that of the monoparticle system, which means the wake effect on the trailing particle becomes bigger. Thus, the drag ratio of the trailing particle is negatively correlated with the wake effect. So, we can identify whether the wake effect weakens by the increase in the drag ratio of the trailing particle.

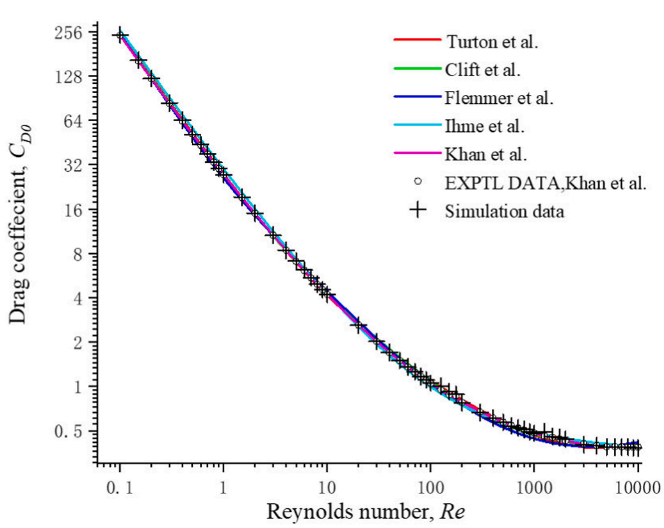

Fig. 3. Drag coefficient as a function of Reynolds number from different sources: Emperical formula: (1) Turton and Levenspiel (1986); (2) Clift and Gauvin (1971); (3) Flemmer et al. (1993); (4) Ihme et al. (1972); (5) Khan and Richardson (1989) experimental data.

3.2.1. Effect of inter-particle distance

The interparticle distance between two particles is a leading factor in influencing the drag force on particles. In this study, the dimensionless interparticle distance L/D (where L is the length of the distance between centers of two particles minus the sum of the diameter of particle, and D is the diameter of particle) is within 0-24, covering three distinct scenarios: strong wake interaction ($L/D = 0$–2), moderate wake interaction ($L/D = 2$–4), and weak wake interaction ($L/D \geq 4$).

To figure out the effect of interparticle distance, in this section, fluid flows through two identical particles, with a Reynolds number of 25 (where wake effect is steady), and a zero angle between them is considered.

It is clearly shown in Fig. 5 that the interparticle distance slightly affects the drag force on the leading particle, while the effect on the drag force of the trailing particle is bigger. According to the figure, the tendency of this research is consistent with the tendency of Chen and Wu (2000) research, which can validate the viability of the Lattice Boltzmann method from another aspect. This figure shows that the drag ratio of the leading particle decreases at the L/D range of 0–1 and increases implicitly. Correspondingly, the drag ratio of the trailing particle keeps increases slower. These trends indicate that the two lines in the figure will get closer and closer, and these lines will tend to 1 eventually.

According to the definition, the condition where the drag ratio is 1 means that the drag force of the particle is equal to that of a monoparticle at the same Reynolds number. In another word, the wake effect on the trailing particle fades. Thus, whether the drag ratio of the trailing particle is 1 or not can be an index to value the wake effect the trailing particle. According to Fig. 5, it can be predicted that the wake effect on the trailing particle is weaker when the interparticle distance between two particles becomes bigger. This phenomenon can be explained by pressure drag and shedding effect.

In multiphase flow systems, pressure drag is the core component of

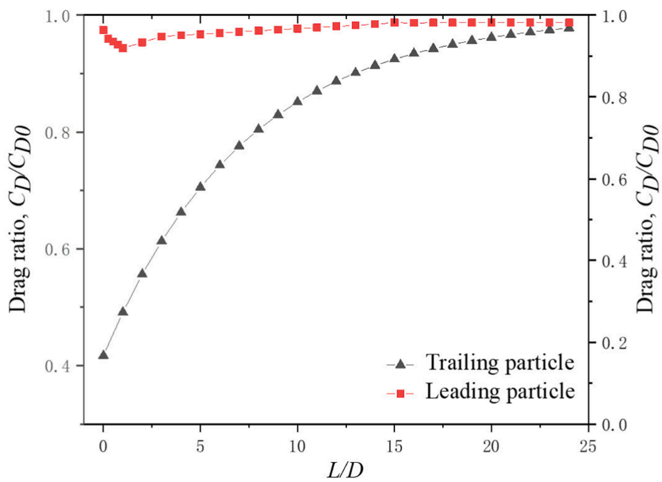

Fig. 5. Drag ratio as a function of different interparticle distance (L/D) when $Re = 25$, $\alpha = 0°$.

particle flow resistance, and the shedding effect is a typical collective flow field effect of dense particle swarms. The coupling of these two effects determines the drag force and transport laws of particles. Pressure drag is induced by the boundary layer separation of fluid flowing around particles, with the pressure difference between the windward and leeward surfaces of particles as its essential generation mechanism, and it dominates when $Re > 10$. Its magnitude follows the classic drag formula and is regulated by particle shape, surface roughness and Re. The particle shedding effect is caused by the spatial occlusion and flow field interference between particles, characterized by the reduction of the effective windward area and local relative velocity of individual particles, leading to the total drag of the particle swarm being less than the arithmetic sum of the drag of isolated particles. This effect includes three forms: flow field shedding, force shedding and near-wall shedding, and its intensity is determined by particle arrangement and Re, which can be quantitatively corrected by the shedding factor. The coupling of the two effects presents a positive feedback mechanism: the shedding effect reduces the local Re and relative velocity, thus weakening the pressure drag; while the wake expansion dominated by pressure drag further strengthens the shedding effect. This coupling characteristic is the core physical mechanism of particle sedimentation, fluidization and other phenomena in dense multiphase flows.

The interparticle distance (L/D) exerts a significant regulatory effect on the pressure drag and vortex shedding effect, especially at $\alpha = 0°$ (maximum wake overlap). When $L/D \leq 2$, the two particles are in close proximity, and their wakes overlap severely: the trailing particle is fully trapped in the leading particle's low-pressure wake, resulting in the minimum pressure drag and suppressed vortex shedding. SCW's high viscosity further enhances this suppression, as viscous dissipation weakens vortex diffusion and wake decay. As L/D increases from 2 to 4, the wake overlap degree decreases gradually: the trailing particle partially moves out of the leading particle's wake, the wake shielding effect weakens, and the pressure drag of the trailing particle increases. When $L/D \geq 4$, The trailing particle escapes the low-pressure wake of the leading particle and the influence of the leading particle on the trailing particle diminishes progressively. So, the wake shielding effect weakens slowly, and the pressure drag of the trailing particle increases slowly. Eventually, the trailing particle exhibits an increasingly similar behavior to an isolated particle in this trend.

3.2.2. *Effect of the interparticle angle between two particles*

If the centerline of two particles is not parallel with the incomming flow direction, the interparticle angle α (α is the angle of the two-particle centerline relative to the incoming flow direction) should be considered. In this section, the dimensionless interparticle distance (L/D) is fixed at 2 (where the leading particle allows ample space for wake vortex development), and the Reynolds number is 20 (where wake effect is steady). Since the range of the interparticle angle (α) between two lines is 0° to 90° (0° and 90° is included), the interparticle angles between two particle is limited to 0°–90° (only 90° is included as 0° has been studied in the former section), covering the scenario where the trailing particle is in the wake of the leading particle ($\alpha = 0°$) to the scenario where the two particles are side-by-side ($\alpha = 90°$), which corresponds to the actual distribution of particles in SCWG reactors. We have also noted that $\alpha = 30°$ and $\alpha = 60°$ are transition points where the wake structure changes from symmetric to asymmetric. Chen and Wu (2000) showed that the effect of the angle of SCW is different from that of ordinary fluid.

In Fig. 5, it clearly displays that the drag ratio of the leading particle is bigger than that of the trailing particle. Besides, when $\alpha = 90°$, the drag ratio of the leading particle is equal to that of the trailing particle. Furthermore, when the interpaticle angles increase, the drag ratio of the trailing particle increases as well, in another word, the leading particle wake effect on the trailing particle is weakening with interparticle angle increasing.

For the leading particle, the drag ratio increases rapidly with the increase of the interparticle angle in the range of $30° \leq \alpha \leq 60°$, but the drag force is less affected by the interparticle angle in the range of $0° < \alpha < 30°$ and $60° < \alpha \leq 90°$. In addition, when the inter-p angles are equal to 90° and the interparticle distance is equal to or greater than 2, the drag ratio is equal to 1, which means the drag force of one particle is scarcely affected by the other particle.

For a trailing particle, in total, the drag ratio of the trailing particle is increasing with the include angle increases. From Fig. 6, we can see that while the interparticle angle is in the range of 0°–45°, the drag ratio increases more rapidly than the drag ratio with the interparticle angle in the range of 45°–90°. Particularly, when the interparticle angle at the interparticle angle of 90°, the drag ratio of the trailing particle is equal to that of the leading particle.

In this case, when the interparticle distance is equal to or more than 2, the drag ratio is equal to 1. The tendency of the drag ratio can also be validated by the figure of streamlines shown in Fig. 7, which depicts the flow lines of the fluid around two identical particles at 30° (a), 60° (b), and 90° (c), respectively. When the interparticle angle increases from 30° to 60°, a wake vortex is formed in the lower right corner of the trailing particle. The interparticle angle increased from 60° to 90°, forming asymmetric wake vortices behind both particles. This phenomenon is related to the relative position of two particles. The leading particle is fixed on the axis of symmetry in the y direction, while the

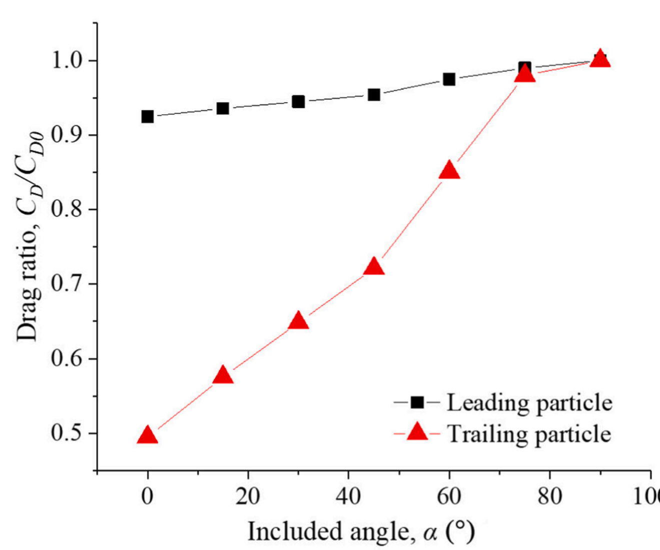

Fig. 6. Drag ratio as a function of interparticle angle α when $L/D = 3$, $Re = 20$.

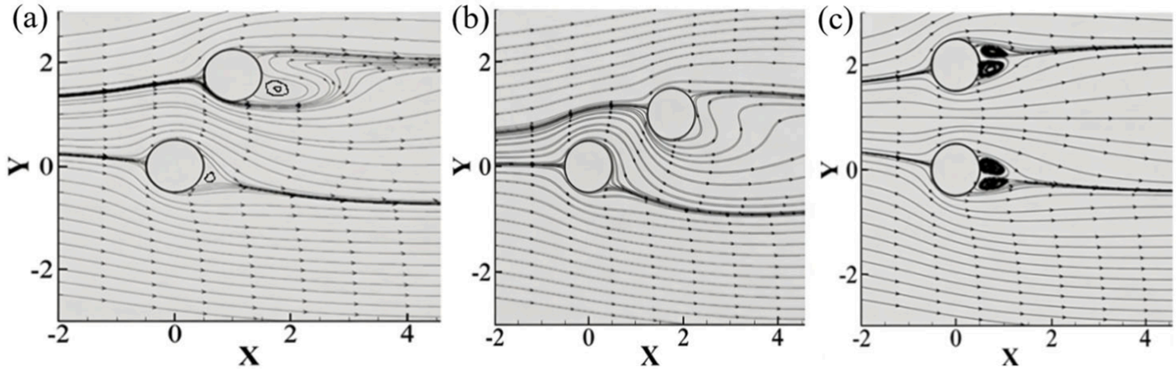

Fig. 7. Streamlines of $\alpha = 30^\circ$ (a), 60° (b), and 90° (c).

trailing particle rotates around the leading particle. Asymmetrical particle distribution results in an asymmetric flow field. When the interparticle angle increases, the streamline behind the trailing particle is severely distorted, resulting in boundary layer separation and wake vortex. Especially, when the interparticle angle is equal to 90°, the streamline of the leading particle and the trailing particle are identical, which indicates the same drag ratio of these particles. The wake effect of the trailing particle weakens when the interparticle angle increases.

3.2.3. Effect of Reynolds number

Supercritical water flow through two particles at different Reynolds numbers (Re = is another aspect of this problem. According to the research of Chen and Wu (2000), Re affects not only the drag forces, but also the effect of interparticle distance on the drag ratio of the trailing particle.

Fig. 8 shows how the drag ratio varies with the Reynolds number varying within the range of 1–200, whose range corresponds to the actual operating conditions of SCWG systems, where the flow of SCW past particles falls within the low-to-moderate Reynolds number range. In total, the drag ratio of the leading particle is bigger than that of the trailing particle. Besides, the drag ratio of the leading particle decreases with increasing Reynolds number, whereas the drag ratio of the trailing particle decreases first and then increases. Moreover, when the Reynolds number increases, the variation of the drag force on the leading particle and the trailing particle is not identical.

The change of drag ratios of two identical particles in the flow field of supercritical water is shown in Fig. 8 According to this figure, the Reynolds number and particle center distance, the drag ratio of the leading particle is much greater than that of the trailing particle. For example, when $Re = 20$, $L/D = 2$, the drag ratios of the leading particle and the trailing particle are 0.971291 and 0.494815, respectively. This is mainly caused by the particle wake effect of the leading particle on the trailing particle. Especially, with the increase of Reynolds number, the drag ratio of the trailing particle decreases and increases in sequence. When the Reynolds number is equal to 92, the drag ratio of the trailing particle begins to turn up after turning down. Since the drag ratio on the trailing particle is a parameter to value the wake effect, we can assert that the wake effect on the trailing particle turns up and down in the figure.

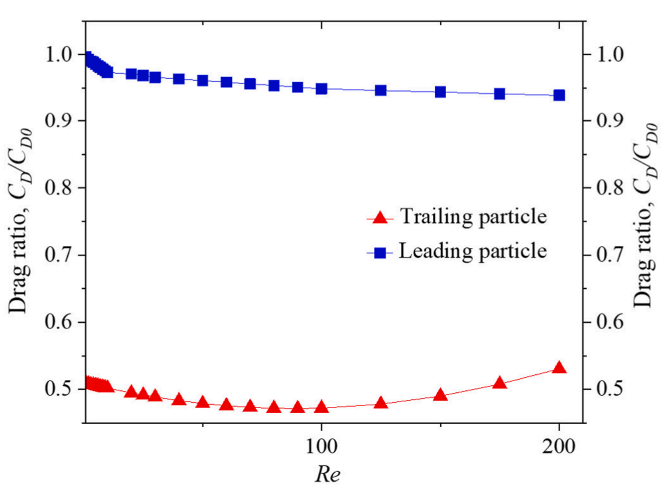

Fig. 8. Drag ratio as a function of Reynolds number Re, when $\alpha = 0^\circ$, $L/D = 3$.

In Fig. 9 the streamlines of different period of Re is shown. At low Re (<50, laminar flow), viscous dissipation dominates, forming a symmetric laminar wake (Fig. 9(a), $Re = 40$) with regular streamlines and no obvious vortex shedding. SCW's high viscosity suppresses wake diffusion, maintaining wake symmetry. For $50 \le Re \le 92$ (laminar-to-transitional flow), inertial force breaks the viscous-inertial balance, causing wake symmetry breaking (Fig. 9(b), $Re = 70$) and initiating weak organized vortex shedding. At $Re = 92$ (critical threshold), symmetry is fully broken, corresponding to the trailing particle's minimum drag coefficient (balance of vortex shedding and viscous suppression). At high Re (>92, transitional flow), inertial force dominates, forming a short, turbulent, highly asymmetric wake (Fig. 9(c), $Re = 120$) with intense, disorganized vortex shedding. SCW's viscosity exerts slight damping but cannot suppress vortex shedding, shortening wake length and weakening shedding effect.

3.2.4. Correlation among drag ratio, interparticle distance, and Re

Since three parameters are difficult to build a correlation and the interparticle angle is not easy to nondimensionalize, interparticle distance and Re are chosen to establish a correlation for darg ratio of the drag ratio in two-particle system. In this section, the drag ratio of the trailing particle as a parameter is correlated with interparticle distance and Re using the data from the simulation. Chen and Wu (2000) established a similar correlation between drag ratio and interparticle distance, Re.

We considered the different condition for various interparticle distances and Re. According to Fig. 10, when $Re < 10$ and $L/D = 1, 2, 4$, the drag ratio of the trailing particle is nearly constant. Still further, with the interparticle distance increasing, the drag ratio of the trailing particle is more constant. When the Reynolds number is more than 10, and the interparticle distance is less than 4 (not included), the drag ratio of the trailing particle turns down first and then turns up. However, when L/D is more than 4 (included) and the Reynolds number is more than 10, the drag ratio of the trailing particle keeps increasing with the increase in Reynolds number. That is because when L/D increases, the drag ratio of the trailing particle increases, and the interparticle distance has a bigger effect on the Reynolds number on the drag ratio of the trailing particle in the Reynolds number range of 1–10.

Firstly, we get an equation for interparticle distance fitting with the

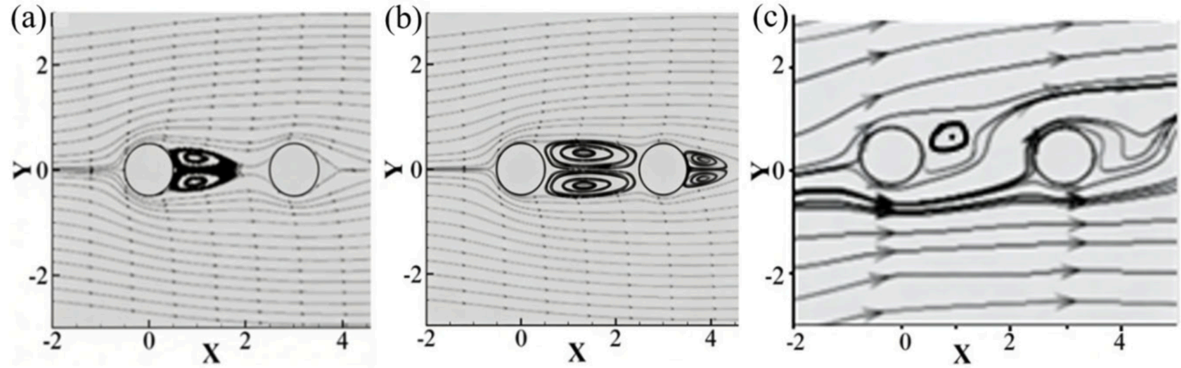

Fig. 9. Streamlines of two-particle system when $Re = 40$ (a), 70 (b), and 120 (c).

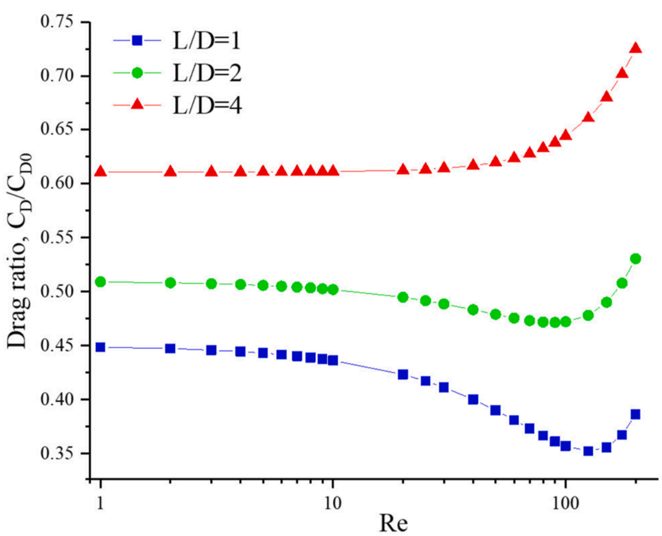

Fig. 10. Drag ratio of the trailing particle as a function of Re when $L/D = 1$, 2, 4, and $\alpha = 0°$.

curve of the drag ratio of the trailing particle in Fig. 5:

$$\frac{C_D}{C_{D0}} = 1 - 0.66802*\mathrm{EXP}\left(-0.13652*\frac{L}{D}\right) \tag{19}$$

then, the data of the drag ratio at $Re = 1$, 150 is simulated. Functions of drag ratio for L/D are established to fit with this data as an equation based on MATLAB R2018a.

$$\frac{C_D}{C_{D0}} = 1 - 0.61906*\mathrm{EXP}\left(-0.11587*\frac{L}{D}\right) \tag{20}$$

$$\frac{C_D}{C_{D0}} = 1 - 0.81363*\mathrm{EXP}\left(-0.23363*\frac{L}{D}\right) \tag{21}$$

Based on Eqs. (12)–(14), we assume that 0.66802 and −0.13652 are functions of Re, A(Re), and B(Re), we can get an equation as Eq. (22):

$$\frac{C_D}{C_{D0}} = 1 - \mathrm{A}(Re)*\mathrm{EXP}\left(\mathrm{B}(Re)*\frac{L}{D}\right) \tag{22}$$

Based on Fig. 8, we notice that when $L/D = 4$, the equation fitting with the curve of Re is as Eq. (23):

$$\frac{C_D}{C_{D0}} = \mathrm{EXP}\left(-0.49489 + 1.93632\mathrm{E}-4\mathrm{Re} + 3.44763\mathrm{E}-6\mathrm{Re}^2\right) \tag{23}$$

thus, we assume that:

$$\mathrm{A}(Re) = 1 - \mathrm{EXP}\left(a_1 + b_1 Re + c_1 Re^2\right) \tag{24}$$

$$\mathrm{B}(Re) = a_2 + b_2 Re + c_2 Re^2 \tag{25}$$

Since there are 6 unknown parameters, 6 equations should be built to get a solution to these unknowns. We substitude datas from Eqs. (23)–(25) to get the following:

$$a_1 + 25b_1 + 625c_1 = -1.10268 \tag{26}$$

$$a_2 + 25b_2 + 625c_2 = -0.13652 \tag{27}$$

$$a_1 + b_1 + c_1 = -0.96510 \tag{28}$$

$$a_2 + b_2 + c_2 = -0.11587 \tag{29}$$

$$a_1 + 150b_1 + 22500c_1 = -1.68002 \tag{30}$$

$$a_2 + 150b_2 + 22500c_2 = -0.23363 \tag{31}$$

According to these equations, we can get a_1 = -0.95918, b_1 = -0.00593, c_1 = 7.47507E-06, a_2 = -0.11500, b_2 = -8.74993e-4, c_2 = 5.60649e-7.

Thus, the correlation of drag ratio for L/D and Re is as follows:

$$\frac{C_D}{C_{D0}} = 1 - \mathrm{A}(Re)*\mathrm{EXP}\left(\mathrm{B}(Re)*\frac{L}{D}\right) \tag{32}$$

where:

$$\mathrm{A}(Re) = 1 - \mathrm{e}^{\left(-0.95918 - 0.00593Re + 7.47507*10^{-6}Re^2\right)} \tag{33}$$

$$\mathrm{B}(Re) = -0.11500 - 8.74993*10^{-4}Re + 5.60649*10^{-7}Re^2 \tag{34}$$

The range of Reynolds numbers is 0.1-200.

In order to validate this correlation, several conditions have been involved to compare the simulation results and the calculation results of this correlation. The comparison results are as Table 1, where S is the simulation results and C is the calculation results.

In Table 1, several random initial conditions have been adopted. According to the comparison in the table, we can see that there is little difference between simulation results and calculation results within a

Table 1
Comparison between simulation results (S) and calculation results (C).

Variables (L/D, Re)	C_D/C_{D0} of S	C_D/C_{D0} of C	Difference of S and C (%)
1,4, 4	0.4702	0.4699	0.64
1.4, 45	0.4310	0.4335	−5.77
1.4, 150	0.4134	0.4133	0.24
6, 4	0.6928	0.6926	0.29
6, 45	0.7188	0.7201	−1.81
6, 150	0.7997	0.7997	0

reasonable error margin of ±10%. Thus, the correlation is validated.

4. Conclusion

This study numerically investigates the particle wake characteristics, wake-particle interaction mechanisms, and numerical simulation methods in high-viscosity supercritical water (SCW) using an adaptive lattice Boltzmann method (LBM), with the aim of providing theoretical and numerical support for supercritical water gasification (SCWG) reactor optimization. Based on the systematic simulation and analysis, the main conclusions are drawn as follows:

(1) The adaptive LBM framework (with a medium grid system of $N/D = 30$, 0.025:0.060 coarse-fine lattice refinement ratio) is proven to be suitable for simulating SCW flow past particles. Compared with non-adaptive uniform lattices, it effectively balances numerical accuracy and computational efficiency and excessive computational cost (uniform fine lattice, cost increased by 70%), and accurately resolves the steep viscosity gradients and fine-scale wake structures in SCW.
(2) The interparticle distance is the leading factor to affect the drag force on particles. The interparticle distance exerts a far greater influence on the drag force of the trailing particle than on that of the leading particle. The result shows three distinct scenarios: strong wake interaction ($L/D = 0$–2), moderate wake interaction ($L/D = 2$–4), and weak wake interaction ($L/D \geq 4$). This is because of pressure drag and shelddding effect. The coupling of these two effects determines the drag force and transport laws of particles. For $L/D \leq 2$, severe wake overlap in SCW traps the trailing particle in the leading one's low-pressure wake, minimizing its pressure drag and suppressing vortex shedding (amplified by SCW's high viscosity). L/D rising to 4 reduces overlap, weakens shielding and increases the trailing particle's pressure drag. At $L/D \geq 4$, the trailing particle escapes the wake, with shielding further diminished and its pressure drag increased, behaving increasingly like an isolated particle.
(3) The drag ratios of two particle increase with the increase of interparticle angle. 30°–60° forms a wake vortex at the trailing particle's lower right; 60°–90° induces asymmetric vortices behind both particles, caused by asymmetric flow from particle rotation, weakening the trailing particle's wake effect, and 90° brings identical drag for both particles.
(4) The wake symmetry and vortex shedding in SCW show a clear Reynolds number (Re)-dependent transition: symmetric laminar wake ($Re < 50$, no obvious vortex shedding), symmetric-asymmetric transition ($50 \leq Re \leq 92$, weak organized vortex shedding), and highly asymmetric turbulent wake ($Re > 92$, intense disorganized vortex shedding). The critical $Re = 92$ is the balance point of viscous suppression and vortex shedding, corresponding to the minimum drag ratio of the trailing particle.
(5) An correlation of drag ratio with L/D and Re is established to calculate the drag ratio of the trailing particle.

In summary, the adaptive LBM proposed in this study provides a robust numerical tool for simulating particle-fluid-particle interaction in high-viscosity SCW. The clarified coupling mechanism of L/D, α, and Re on wake characteristics, wake shielding effect, and pressure drag offers important theoretical guidance for the optimization of SCWG reactor internal structure, particle feeding mode, and operational parameters. Future work will focus on expanding the simulation to particle swarms and validating the numerical results with experimental data to further improve the engineering applicability of the research.

CRediT authorship contribution statement

Xue Qiao: Writing – original draft, Investigation. **Hui Jin:** Writing – review & editing. **Haozhe Su:** Writing – review & editing. **Liejin Guo:** Project administration, Funding acquisition.

Declaration of competing interest

The authors declare that they have no known competing financial interests or personal relationships that could have appeared to influence the work reported in this paper.

Acknowledgment

This work is supported by the Basic Science Center Program for Ordered Energy Conversion of the National Natural Science Foundation of China (grant No. 52488201).

References

Chen, S., & Doolen, G. D. (1998). Lattice boltzmann method for fluid flows. *Annual Review of Fluid Mechanics, 30*, 329–364.
Chen, R. C., & Wu, J. L. (2000). The flow characteristics between two interactive spheres. *Chemical Engineering Science, 55*, 1143–1158.
Clift, R., & Gauvin, W. H. (1971). Motion of entrained particles in gas streams. *Canadian Journal of Chemical Engineering, 49*, 439-&.
Dupuis, A., & Chopard, B. (2003). Theory and applications of an alternative lattice boltzmann grid refinement algorithm. *Physical Review E, 67*.
Filippova, O., & Hänel, D. (2000). Acceleration of lattice-BGK schemes with grid refinement. *Journal of Computational Physics, 165*, 407–427.
Filippova, O., Schwade, B., & Hänel, D. (2002). Multiscale lattice boltzmann schemes for low mach number flows. *Philosophical Transactions of the Royal Society of London Series a-Mathematical Physical and Engineering Sciences, 360*, 467–476.
Flemmer, R. L. C., Pickett, J., & Clark, N. N. (1993). An experimental-study on the effect of particle-shape on fluidization behavior. *Powder Technology, 77*, 123–133.
Ihme, F., Schmidtt, H., & Brauer, H. (1972). Thereotical studies on mass-transfer at and flow past spheres. *Chemie Ingenieur Technik, 44*, 306-&.
Jin, H., Lu, Y. J., Liao, B., Guo, L. J., & Zhang, X. M. (2010). Hydrogen production by coal gasification in supercritical water with a fluidized bed reactor. *International Journal of Hydrogen Energy, 35*, 7151–7160.
Jin, H., Wang, H. B., Wu, Z. Q., Ren, Z. H., & Ou, Z. S. (2019). Numerical investigation on drag coefficient and flow characteristics of two biomass spherical particles in supercritical water. *Renewable Energy, 138*, 11–17.
Khan, A. R., & Richardson, J. F. (1989). Fluid-particle interactions and flow characteristics of fluidized-beds and settling suspensions of spherical-particles. *Chemical Engineering Communications, 78*, 111–130.
Kretzschmar, H. J., Cooper, J. R., Gallagher, J. S., Harvey, A. H., Knobloch, K., Mares, R., Miyagawa, K., Okita, N., Span, R., Stocker, I., Wagner, W., & Weber, I. (2007). Supplementary backward equations p(hs) for the critical and supercritical regions (region 3), and equations for the two-phase region and region boundaries of the IAPWS industrial formulation 1997 for the thermodynamic properties of water and steam. *Journal of Engineering for Gas Turbines and Power-Transactions of the Asme, 129*, 1125–1137.
Kretzschmar, H. J., Harvey, A. H., Knobloch, K., Mareš, R., Miyagawa, K., Okita, N., Span, R., Stöcker, I., Wagner, W., & Weber, I. (2009). Supplementary backward equations v(p,T) for the critical and supercritical regions (region 3) of the IAPWS industrial formulation 1997 for the thermodynamic properties of water and steam. *Journal of Engineering for Gas Turbines and Power, 131*, 1–16.
Ladd, A. J. C. (1994). Numerical simulations of particulate suspensions via a discretized boltzmann-equation. *Journal of Fluid Mechanics, 271*, 285–309.
Li, X., Ouyang, J., Wang, X. D., & Chu, P. P. (2021). A drag force formula for heterogeneous granular flow systems based on finite average statistical method. *Particuology, 55*, 94–107.
Liu, X. L., & Guo, Z. L. (2013). A lattice boltzmann study of gas flows in a long micro-channel. *Computers & Mathematics with Applications, 65*, 186–193.
Liu, J. C., Zhang, Y. Q., Yin, Q. L., Liu, Q. S., Ding, S. H., Xing, Y. W., & Gui, X. H. (2024). Experimental study of hydrodynamic characteristics in three-phase coarse particle fluidized flotation column. *Chemical Engineering Journal, 500*.
Taneda, S. (1956). Experimental investigation of the wake behind a sphere at low Reynolds numbers. *Journal of the Physical Society of Japan, 11*, 1104–1108.
Tsuji, T., Narutomi, R., Yokomine, T., Ebara, S., & Shimizu, A. (2003). Unsteady three-dimensional simulation of interactions between flow and two particles. *International Journal of Multiphase Flow, 29*, 1431–1450.
Turton, R., & Levenspiel, O. (1986). A short note on the drag correlation for spheres. *Powder Technology, 47*, 83–86.
Wagner, W., Cooper, J. R., Dittmann, A., Kijima, J., Kretzschmar, H. J., Kruse, A., Mares, R., Oguchi, K., Sato, H., Stocker, I., Sifner, O., Takaishi, Y., Tanishita, I., Trubenbach, J., & Willkommen, T. (2000). The IAPWS industrial formulation 1997 for the thermodynamic properties of water and steam. *Journal of Engineering for Gas Turbines and Power-Transactions of the Asme, 122*, 150–182.
Wang, Y., Shu, C., Huang, H. B., & Teo, C. J. (2015). Multiphase lattice boltzmann flux solver for incompressible multiphase flows with large density ratio. *Journal of Computational Physics, 280*, 404–423.

Wang, X., & You, C. F. (2011). Evaluation of drag force on a nonuniform particle distribution with a meshless method. *Particuology, 9*, 288–297.

Wei, L. P., & Lu, Y. J. (2016). Fluidization of solids with water in supercritical conditions - Characteristics of pressure fluctuations. *Chemical Engineering Research and Design, 109*, 657–666.

Wei, L. P., Lu, Y. J., & Wei, J. J. (2014). Numerical study on laminar free convection heat transfer between sphere partical and high pressure water in pseudo-critical zone. *Thermal Science, 18*, 1293–1303.

Wu, W., Zhu, M. F., Sun, D. K., Dai, T., Han, Q. Y., & Raabe, D. (2012). Modelling of dendritic growth and bubble formation. In *13th international conference on modeling of casting, welding and advanced solidification processes (MCWASP)*. AUSTRIA: Schladming.

Xiang, N., Yi, H., Chen, K., Sun, D. K., Jiang, D., Dai, Q., & Ni, Z. H. (2013). High-throughput inertial particle focusing in a curved microchannel: Insights into the flow-rate regulation mechanism and process model. *Biomicrofluidics, 7*.

Yu, Z., & Fan, L. S. (2010). Lattice boltzmann method for simulating particle-fluid interactions. *Particuology, 8*, 539–543.

Zhang, J., & Fan, L. S. (2002). A semianalytical expression for the drag force of an interactive particle due to wake effect. *Industrial & Engineering Chemistry Research, 41*, 5094–5097.

Zhang, Y. C., Ozalp, N., & Xie, G. N. (2019). LBM modelling unsteady flow past and through permeable diamond-shaped cylinders effects of aspect ratios and darcy numbers. *International Journal of Numerical Methods for Heat and Fluid Flow, 29*, 3472–3497.

Zhang, H., Xiong, B., An, X. Z., Ke, C. H., & Chen, J. (2020). Numerical prediction on the drag force and heat transfer of non-spherical particles in supercritical water. *Powder Technology, 361*, 414–423.

Zhang, M. Y., Zhao, Q. Y., Huang, Z. J., Chen, L., & Jin, H. (2021). Numerical simulation of the drag and heat-transfer characteristics around and through a porous particle based on the lattice boltzmann method. *Particuology, 58*, 99–107.

Zhu, C., Guo, L. J., Jin, H., Ou, Z. S., Wei, W. W., & Huang, J. B. (2018). Gasification of guaiacol in supercritical water: Detailed reaction pathway and mechanisms. *International Journal of Hydrogen Energy, 43*, 14078–14086.

Zhu, C., Liang, S. C., & Fan, L. S. (1994). Particle wake effects on the drag force of an interactive particle. *International Journal of Multiphase Flow, 20*, 117–129.